Copyright © 2007 by ABCM

TOPOLOGY OPTIMIZATION OF PLATE-LIKE STRUCTURES WITH RESPECT TO ACOUSTIC RADIATION

F. H. Mendonça
DEM, Instituto Superior Técnico, Portugal

O. M. Silva, olavo@lva.ufsc.br
GTVA, Federal University of Santa Catarina, Florianópolis, Brazil

M. M. Neves, maneves@dem.ist.utl.pt
IDMEC, Instituto Superior Técnico, Portugal

F. J. P. Lau, lau@dem.ist.utl.pt
CCTAE, Instituto Superior Técnico, Portugal

Abstract. *This paper investigates the minimization and maximization of the acoustic radiation from a vibrating plate-like structure by applying a topology optimization method for bi-material structures. The optimization is based on the Method of Moving Asymptotes (MMA) and a combination of both MatLab® algorithms and the ANSYS® commercial finite element software. Optimization for reducing the radiated sound is carried out for a plate subjected to a uniformly distributed pressure and point forces at specific frequencies. From the obtained results, sound power flow reductions of up to 99% are achieved for the distributed and point loadings. Higher frequencies yield the most complex topologies and are, therefore, the most difficult to optimize. The behaviour of the new design sets is checked in a wide frequency range ([1, 2000] Hz), showing both positive and negative impacts; shift, suppression or addition of radiation peaks are the most notable results of the structural modifications. Maximization is investigated for the uniform pressure loading only, with improvements of up to 2057%.*

Keywords*: topology optimization, acoustic radiation, distributed load, plate-like structures.*

1. INTRODUCTION

Noise control by design has been acquiring a greater importance every day. The reduction of low frequency noise is of particular interest, not only because of comfort–related issues, but also because this is usually the most difficult range to deal with. Although active vibration control could be used, passive vibration control remains the simplest, cheapest and most reliable mean of reducing radiated noise, especially when excitation have few frequencies and because the treatment is applied directly to the sources.

Mechanical constraints, like those investigated by Ming *et al*. (2000), may be applied to structures to convert uniform effective vibrating shapes to irregular and ineffective ones, thus reducing the total vibration level. Consequently, harmonic structural vibration is suppressed and the tonal noise radiation reduced. Also, the conversion of mode shapes of a vibrating shell into weak radiators can be accomplished through the introduction of point masses and the calculation of their optimal distributions, as was done by Constans *et al*. (1998). Bös (2006) investigated a method to optimize the thickness distribution of three–dimensional structures with respect to various structural and vibrational properties such as the structure-borne sound or vibration levels, structural mass and fundamental frequencies. Luo and Gea (2003) also based their approach on topology optimization in order to find optimal stiffeners configuration to reduce interior noise, treating the problem as a material distribution problem.

The present work focuses on the topology optimization of a bi-material plate–like structure with respect to noise radiation as proposed by Olhoff and Du (2007). The sound power flow from the surface is reduced or maximized by adding mass to or removing mass from key elements using two materials with very distinct properties, allowing the structure's boundary shape to remain unchanged. Such mass re–arrangements optimize the structural response to the applied loadings. No damping effects are considered. For the optimization to take place, one has to be able to measure the structural-borne radiation. Although this may be done in different ways, e.g. knowing the sound pressure or pressure level, directly provided by a finite element software, or the sound power level, as shown in the work by Herrin *et al*. (2006), the sound power flow reveals itself as the most adequate mean for quantifying the radiation at the structure's surface.

2. SOUND POWER FLOW FROM A VIBRATING STRUCTURE

The time–harmonic surface load $p(t)$ applied to the structure and the displacement response vector $u(t)$ are in–phase if no damping is assumed and there is a weak coupling between the structure and the medium, and are therefore expressed as

$$p(t) = Pe^{-i\omega_p t} \quad \text{and} \quad u(t) = Ue^{-i\omega_p t}\,, \tag{1}$$

where ω_p is the prescribed forcing frequency (expressed in rad/s) and P and U the load and displacement amplitudes. If the forcing frequency is considered to be high enough, the radiation impedance at the structure's boundary is approximately the same as the characteristic impedance of the acoustic medium. Thus, the acoustic pressure p_f and the normal velocity v_n of the structural surface approximately relate through $p_f = \gamma_f c v_n$, in which c represents the speed of sound and γ_f the specific mass or mass density of the acoustic medium.

The finite element formulation for the problem of the vibrating structure, subjected to both external mechanical and acoustic loadings, is expressed as

$$\left[K - \omega_p^2 M\right]U = P + LP_f\,, \tag{2}$$

where K, M and L denote the stiffness, mass and fluid–structure coupling matrices, respectively; U represents the structural displacement response vector for the applied load at the prescribed forcing frequency ω_p; P and P_f are the vectors of amplitudes of the mechanical loading and acoustic pressure on the structure's surface, respectively. Since weak coupling between the structure and the acoustic medium is assumed (which is more than reasonable for air and wide or open spaces), the problem reduces to a vibrating structure under a mechanical loading P only and the term LP_f in Eq. (2) is disregarded.

The sound power flow Π may be obtained by integrating the acoustic intensity along an imaginary spherical surface and having the above simplifications in mind, which yields the following expression (for further details see Olhoff and Du, 2007):

$$\Pi = \frac{1}{2}\gamma_f c\omega_p^2 U^T S_n U\,. \tag{3}$$

The surface normal matrix S_n depends on the finite element's shape function matrix N and the unit normal n (unit vector perpendicular to the undeformed structure's surface at the centroid of each finite element) and is expressed as

$$S_n = \sum_{e=1}^{N} S_{ne} = \sum_{e=1}^{N}\left(\int_{S_e} N^T nn^T N dS\right). \tag{4}$$

3. TOPOLOGY OPTIMIZATION OF BI-MATERIAL STRUCTURES

Topological design optimization is considered in this section with the goal of minimizing (or maximizing) the total sound power flow of the structure. This will be considered a bi-material design problem, in which an optimal distribution of two different materials is achieved for the minimum sound radiation.

A complete formulation of the problem of minimizing the sound power flow Π is presented by Olhoff and Du (2007) as follows:

$$\min_{\rho_e} \quad \left\{\Pi = \frac{1}{2}\gamma_f c\omega_p^2 U^T S_n U\right\} \tag{5}$$

subject to

$$\begin{gathered}\left[K - \omega_p^2 M\right]U = P,\\ \sum_{e=1}^{N_E}\rho_e V_e - V_1 \le 0,\ V_1 = \alpha V_0 \quad \text{and} \quad 0 \le \rho_e \le 1,\ e = 1,...,N_E\,,\end{gathered} \tag{6}$$

where U and P are the structural displacement and mechanical loading vectors. Note that the fluid–structure coupling is disregarded, as previously referred, hence $LP_f = 0$ in the upper expression of Eq. (6). The volumetric density of the stiffer material in each finite element e is denoted by ρ_e and the set of these values will be the design variable for the optimization. A value of 1.0 for ρ_e means the finite element e fully consists of the stiffer material and, for a value of 0.0, it is entirely made of the softer material; if $0.0 < \rho_e < 1.0$ the element is composed of a mixture of both materials which follows a modified version of the SIMP model (as presented in section 3.2). V_e is the volume of each finite element; α is

the maximum fraction of stiffer material in the structure, thus V_1 is the maximum allowable amount of stiffer material in the design domain of total volume V_0; and N_E denotes the total number of elements.

3.1. Sensitivity Analysis

The topology optimization methodology used here requires the knowledge of the objective function's sensitivity with respect to the design variable, which is obtained from Eq. (3) and using Eq. (2) with the adjoint method.

Applying the partial derivative to Eq. (3), with respect to ρ_e, yields

$$\frac{\partial \Pi}{\partial \rho_e} = \frac{1}{2}\gamma_f c\omega_p^2 \left[\frac{\partial U^T}{\partial \rho_e} S_n U + U^T \left(\frac{\partial S_n}{\partial \rho_e} U + S_n \frac{\partial U}{\partial \rho_e} \right) \right]. \tag{7}$$

The first and third terms at the right side of Eq. (7) are equal and the second one is zero, since S_n is design independent, that is,

$$\frac{\partial U^T}{\partial \rho_e} S_n U = U^T S_n \frac{\partial U}{\partial \rho_e} \text{ and } \frac{\partial S_n}{\partial \rho_e} = 0 \quad \Rightarrow \quad \frac{\partial \Pi}{\partial \rho_e} = \gamma_f c\omega_p^2 \frac{\partial U^T}{\partial \rho_e} S_n U \,. \tag{8}$$

Further re–arrangements to Eq. (8) are made by employing the following auxiliary equation,

$$\left[K - \omega_p^2 M \right] U_s = S_n U \,, \tag{9}$$

where the product S_nU and U_s may be understood as a pseudo load vector and an auxiliary displacement vector, respectively, and by also using the partial derivative of Eq. (2),

$$\frac{\partial U^T}{\partial \rho_e} \left[K - \omega_p^2 M \right] = \frac{\partial P}{\partial \rho_e} - \left[\frac{\partial K}{\partial \rho_e} - \omega_p^2 \frac{\partial M}{\partial \rho_e} \right] U \,. \tag{10}$$

Applying Eqs. (9) and (10) to Eq. (8) will result in the final expression for the sensitivity of the sound power flow:

$$\frac{\partial \Pi}{\partial \rho_e} = \gamma_f c\omega_p^2 \frac{\partial U^T}{\partial \rho_e} \left(K - \omega_p^2 M \right) U_s \quad \Rightarrow \quad \Pi' = \gamma_f c\omega_p^2 \left[U_s^T P' - U_s^T \left(K' - \omega_p^2 M' \right) U \right]. \tag{11}$$

The prime denotes partial derivative with respect to ρ_e. Since the mechanical loading P is design–independent, the later equation reduces to (Olhoff and Du, 2007)

$$\Pi' = -\gamma_f c\omega_p^2 U_s^T \left(K' - \omega_p^2 M' \right) U \,. \tag{12}$$

U_s is calculated from Eq. (9) once the nodal displacements (U) are known.

In order to assure the accuracy and verify the algorithms developed for the required sensitivity analyses, the error between the analytical values of Π' and those calculated through finite differences was checked. Confirmation were taken based on the small deviation between the analytical sensitivity, calculated using Eq. (12), and an approximate sensitivity, computed from central finite differences

$$\Pi' = \frac{\Pi\left(\rho_{e\,\text{init}} + incr_\rho \right) - \Pi\left(\rho_{e\,\text{init}} - incr_\rho \right)}{2 \times incr_\rho}, \; \rho_{e\,\text{init}} = 0.5 \,, \tag{13}$$

for various increments $incr_\rho$.

3.2. SIMP Model for Topology Optimization of Bi-Material Structures

The sensitivities for the stiffness and mass matrices, K' and M' in Eq. (12), may be computed by modifying the Solid Isotropic Material with Penalization (SIMP) model for single–material designs (Bendsøe and Sigmund, 1999) to a bi–material interpolation (Olhoff and Du, 2007):

$$K_{De}(\rho_e) = \rho_e^n K_{De}^1 + \left(1-\rho_e^n\right) K_{De}^2 \quad \text{with} \quad K_D = \left[K - \omega_p^2 M \right]. \tag{14}$$

The penalization power n applied to the dynamic stiffness K_D (that is, to both stiffness and mass) is adjusted in order to define how fast each element shifts to the stiffer or softer material; $n = 3$ is high enough so to avoid intermediate materials ($0.0 < \rho_e < 1.0$) as much as possible, that is, intermediate densities are being sufficiently penalized, in order to achieve the desired black–and–white design sets.

4. OPTIMIZATION SCHEME

The optimization scheme is represented in Fig. 1. It consists of feeding an external MMA optimizer with all the necessary structural response data for the optimization which is provided by the commercial finite element software ANSYS®. The interface between both is established through an additional algorithm, also developed in the MatLab environment.

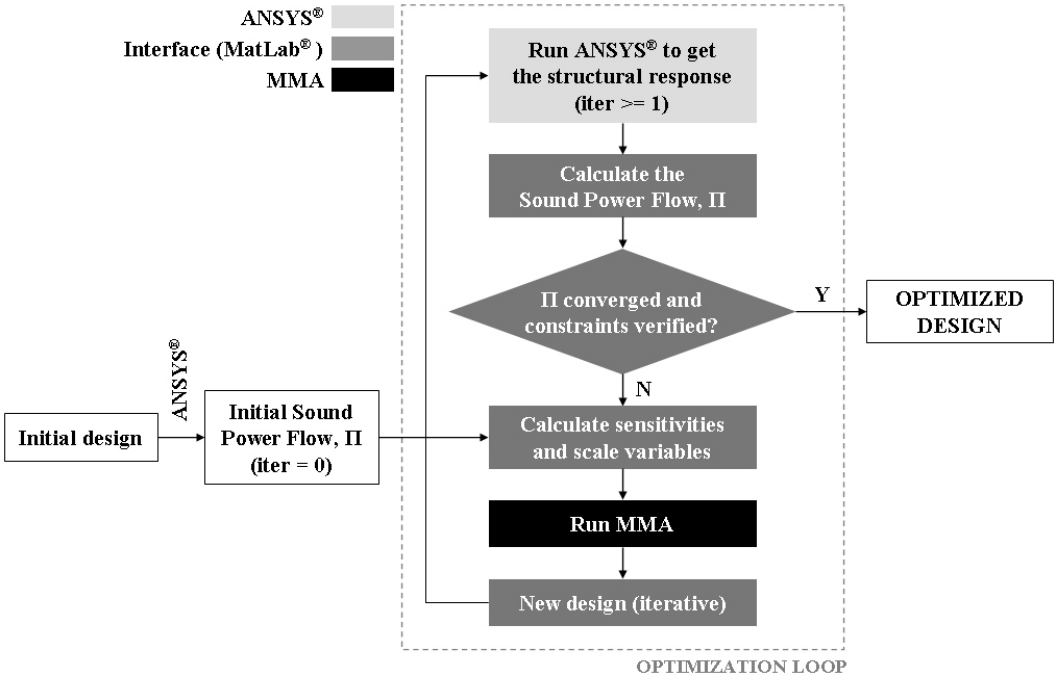

Figure 1. Optimization scheme

The MMA optimizer solves nonlinear optimization problems through an iterative process, where a convex approximation to the original problem is generated and solved in each iteration. Such process is controlled by moving asymptotes which are responsible for stabilizing and accelerating the convergence to a solution (for more details see Svanberg, 1987).

Using ANSYS® makes it possible to save precious code programming time related to the finite element formulations. Both the MMA optimizer and the interface allow working with a considerably higher number of design variables, reduce the overall optimization time (Carvalho *et al*., 2006) and are highly customizable, making it easy to change important optimization parameters or the formulations of the problem itself. The FMINCON (Find MINimum of a CONstrained multivariable function), already implemented in MatLab, was also tested but put aside given the much longer computation times.

5. RESULTS

The results presented next concern the topology optimization of a 2.0×2.0×0.1 m square plate (see Fig. 2) with clamped edges, with an initial value of 0.5 for the design variable ρ_e (uniform throughout the plate). The bi–material structure was modelled by a mesh composed of 40×40×1 shell 8–node isoparametric finite elements SHELL99 (refer to the ANSYS Theory Reference, 2004, for more information). The stiffer material 1 has a Young modulus of 100 GPa, a density of 7800 kg/m^3 and a Poisson ratio of 0.3; the same properties for the softer material 2 are 10 GPa, 780 kg/m^3 and 0.3, respectively.

Optimized design sets were computed for both minimization and maximization of the sound power flow for six different loading frequencies ω_p: 10, 100, 1000, 3000, 5000 and 7000 rad/s. Application of both uniform pressure loading and point forces (centred and deviated from the plate's centre) was investigated during the sound radiation minimization analysis; radiation maximization was investigated for the case of a uniform pressure loading only.

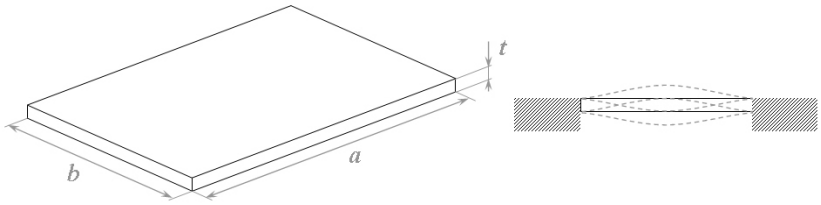

Figure 2. Schematics of the clamped plate with $a = b = 2.0$ m and $t = 0.1$ m

5.1. Minimization of the Sound Power Flow

Tables 1 to 3 present the results obtained for the sound power flow and stiffer material volume for the initial and optimized designs. Reductions of the sound power flow from 32% to 99% were achieved. The improvements are, in general, smaller for the case of uniformly distributed pressure, where every finite element of the plate is under load. Lower reductions are obtained for the centred point force at $\omega_p = 3000$ rad/s and for the point force deviated from the centre at $\omega_p = 10$ and 100 rad/s (Tables 2 and 3), when compared to the same frequencies for the uniform pressure (Table 1).

Although a constraint of 50% was imposed for the fraction of stiffer material during the optimization, an amount of 40% or less was actually obtained for all new design sets, exception made for the deviated point force at $\omega_p = 7000$ rad/s, where that value reached 48%. For this case, a considerable amount of grey elements persisted and the iterative process converged to a solution which actually increases the sound power flow; it was also observed that the optimization gets increasingly oscillatory. An intermediate design set, leading to a radiation reduction of 92%, was therefore considered.

Fractions of 40% of stiffer material were achieved for the uniform pressure and centred point force loadings at $\omega_p = 7000$ and 1000 rad/s, respectively. The fact that the quantity of stiffer material does not come close to the imposed limit also suggests that the constraint may be de–activated.

Table 1. Sound power flow and stiffer material volume
for the initial and optimized designs, uniformly distributed pressure loading

ω_p (rad/s)	f_p (Hz)	Π_{init} (W)	Π_{opt} (W)	Reduction (%)	Stiffer material volume (%)
10	1.59	1.08e-07	1.75e-08	84	36
100	15.9	1.13e-05	1.87e-06	83	36
1000	159	4.91e-05	3.33e-05	32	32
3000	477	9.65e-05	8.63e-06	91	38
5000	796	6.17e-05	2.96e-06	95	30
7000	1114	2.96e-06	1.40e-06	53	40

Table 2. Sound power flow and stiffer material volume
for the initial and optimized designs, centred point force loading

ω_p (rad/s)	f_p (Hz)	Π_{init} (W)	Π_{opt} (W)	Reduction (%)	Stiffer material volume (%)
10	1.59	5.79e-10	4.57e-11	92	36
100	15.9	6.05e-08	4.88e-09	92	36
1000	159	3.72e-06	1.32e-07	96	40
3000	477	1.80e-06	3.39e-07	81	36
5000	796	2.58e-06	6.91e-08	97	38
7000	1114	1.08e-05	2.57e-07	98	29

Table 3. Sound power flow and stiffer material volume
for the initial and optimized designs, point force loading deviated from centre

ω_p (rad/s)	f_p (Hz)	Π_{init} (W)	Π_{opt} (W)	Reduction (%)	Stiffer material volume (%)
10	1.59	5.29e-11	2.13e-11	60	37
100	15.9	5.40e-09	2.27e-09	58	37
1000	159	3.80e-05	3.08e-07	99	34
3000	477	2.71e-06	1.25e-07	95	38
5000	796	2.19e-06	1.09e-07	95	28
7000	1114	1.28e-06	9.81e-08	92	48

Figures 3, 5 and 7 show the mode shapes of the vibrating plate for the six frequencies and different loadings: uniformly distributed pressure, centred point force ($x=a/2$, $y=b/2$) and point force deviated from the centre (located at $x=(3/4)a$, $y=b/2$); black color indicates the maximum/minimum displacements. The optimized topologies for each of the analyzed frequencies are presented in Figs. 4, 6 and 8: black and white color elements are solely composed of the stiffer and softer materials, respectively; grey elements are composed of a mixture between both materials, with $0.0 < \rho_e < 1.0$.

It is clear that, as the frequency increases, the deformed shapes and, consequently, the new topologies get more complex. Adjustments to the finite element mesh should therefore be made by increasing the number of elements per length, which intensifies the level of detail. For the lower frequencies ω_p = 10, 100 and 1000 rad/s the stiffer material is simply placed at the locations where the displacements are highest, that is, at the centre of the plate, for the uniform pressure and centred point force loadings, or near the centre, in the case of the deviated point force. When optimizing for the higher frequencies, a distribution of stiffer material which does not necessarily match the highest displacements is obtained; the complexity of the later designs also leads to some 'point masses', isolated black color elements fully consisted of stiffer material (see Figs. 4e and f, Fig. 6f and Figs. 8d, e and f). This same complexity will also depend on the type of loading applied to the structure: optimization for uniformly distributed pressures will result in less complicated topologies; for the point forces, where all the structural nodes move freely except at the loading point, less achievable and possibly asymmetrical designs are generated, especially for the case of the point force loading deviated from the centre. Such issue may also be overcome through an increase of the number of elements of the finite element mesh. Obtaining simpler design sets may be of great importance from a manufacturability point of view, even if the primary objective of reducing the structure–borne radiation is successfully accomplished.

Some convergence issues arose for the higher frequencies, particularly for the point force deviated from the centre at ω_p = 7000 rad/s (for which case a refined mesh of 60×60×1 elements was used). The new topology presented for the later is the result of a local minimum (see Fig. 8f), not free of grey elements composed of intermediate materials and far from a desired 2–color, black–and–white design. The iterative process converged to a solution which actually increases the sound power flow, a problem that should be subjected to further investigation.

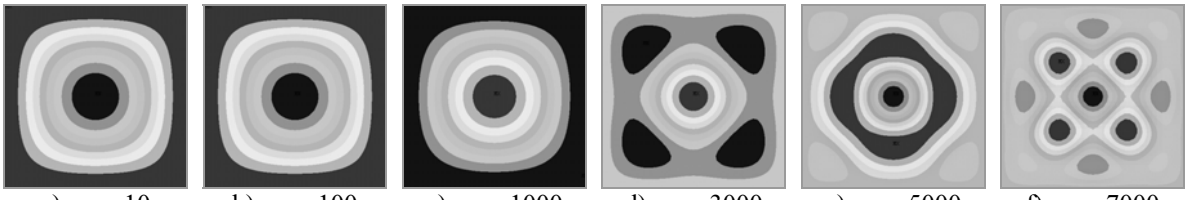

a) ω_p = 10 b) ω_p = 100 c) ω_p = 1000 d) ω_p = 3000 e) ω_p = 5000 f) ω_p = 7000

Figure 3. Mode shapes of the vibrating plate for the initial design,
uniformly distributed pressure loading (ω_p expressed in rad/s)

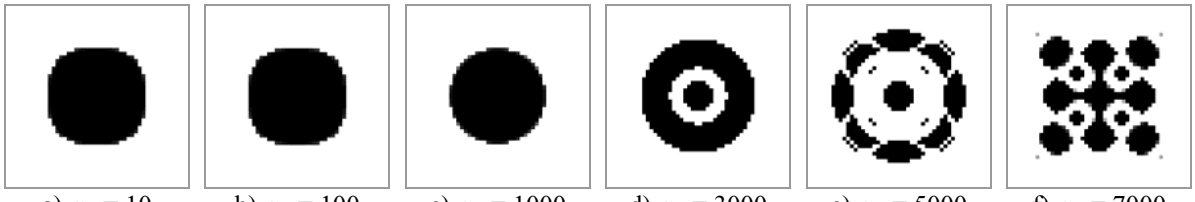

a) ω_p = 10 b) ω_p = 100 c) ω_p = 1000 d) ω_p = 3000 e) ω_p = 5000 f) ω_p = 7000

Figure 4. Optimized topologies for the specific frequencies,
uniformly distributed pressure loading (ω_p expressed in rad/s)

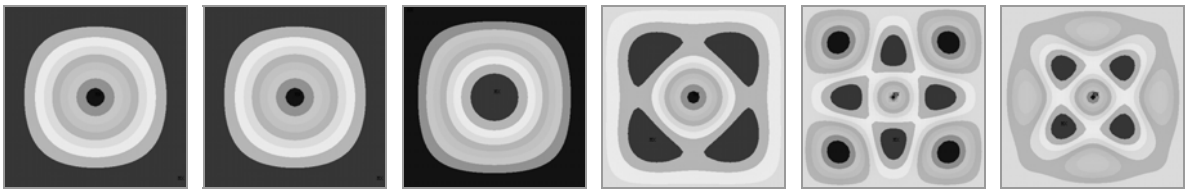

a) $\omega_p = 10$ b) $\omega_p = 100$ c) $\omega_p = 1000$ d) $\omega_p = 3000$ e) $\omega_p = 5000$ f) $\omega_p = 7000$

Figure 5. Mode shapes of the vibrating plate for the initial design, centred point force loading (ω_p expressed in rad/s)

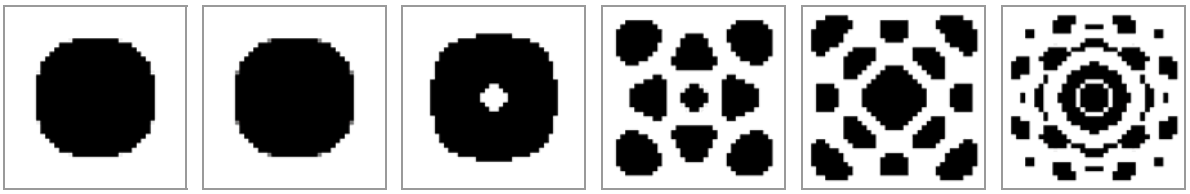

a) $\omega_p = 10$ b) $\omega_p = 100$ c) $\omega_p = 1000$ d) $\omega_p = 3000$ e) $\omega_p = 5000$ f) $\omega_p = 7000$

Figure 6. Optimized topologies for the specific frequencies, centred point force loading (ω_p expressed in rad/s)

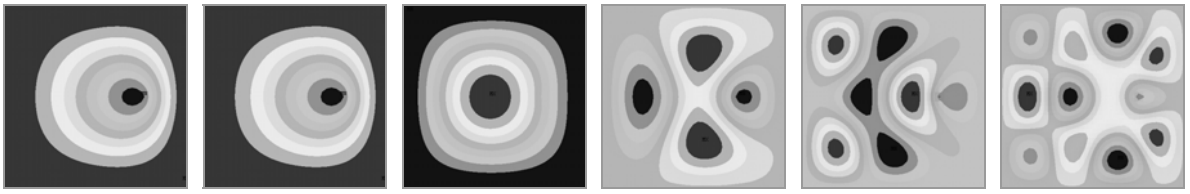

a) $\omega_p = 10$ b) $\omega_p = 100$ c) $\omega_p = 1000$ d) $\omega_p = 3000$ e) $\omega_p = 5000$ f) $\omega_p = 7000$

Figure 7. Mode shapes of the vibrating plate for the initial design, point force loading deviated from centre (ω_p expressed in rad/s)

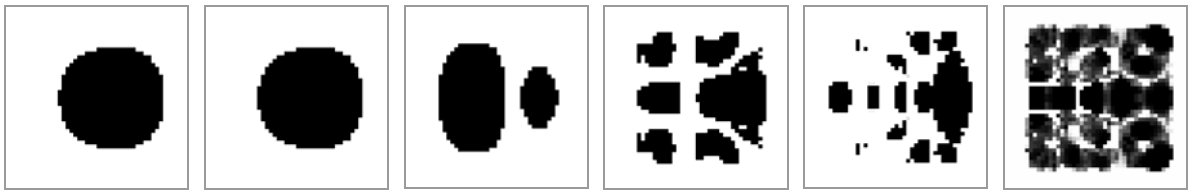

a) $\omega_p = 10$ b) $\omega_p = 100$ c) $\omega_p = 1000$ d) $\omega_p = 3000$ e) $\omega_p = 5000$ f) $\omega_p = 7000$

Figure 8. Optimized topologies for the specific frequencies, point force loading deviated from centre (ω_p expressed in rad/s)

Structural frequency responses in the [1, 2000] Hz range (sound power flow vs. frequency), for the initial and optimized designs, are included in Figs. 9 to 11. Sound power flow minima were obtained for all new design sets not only around the optimization frequency ω_p (marked with a vertical line) but also for other frequency ranges. Positive and negative impacts of the new design sets on the frequency response are best viewed through the depth and width of the spectra's valleys, before and after optimization.

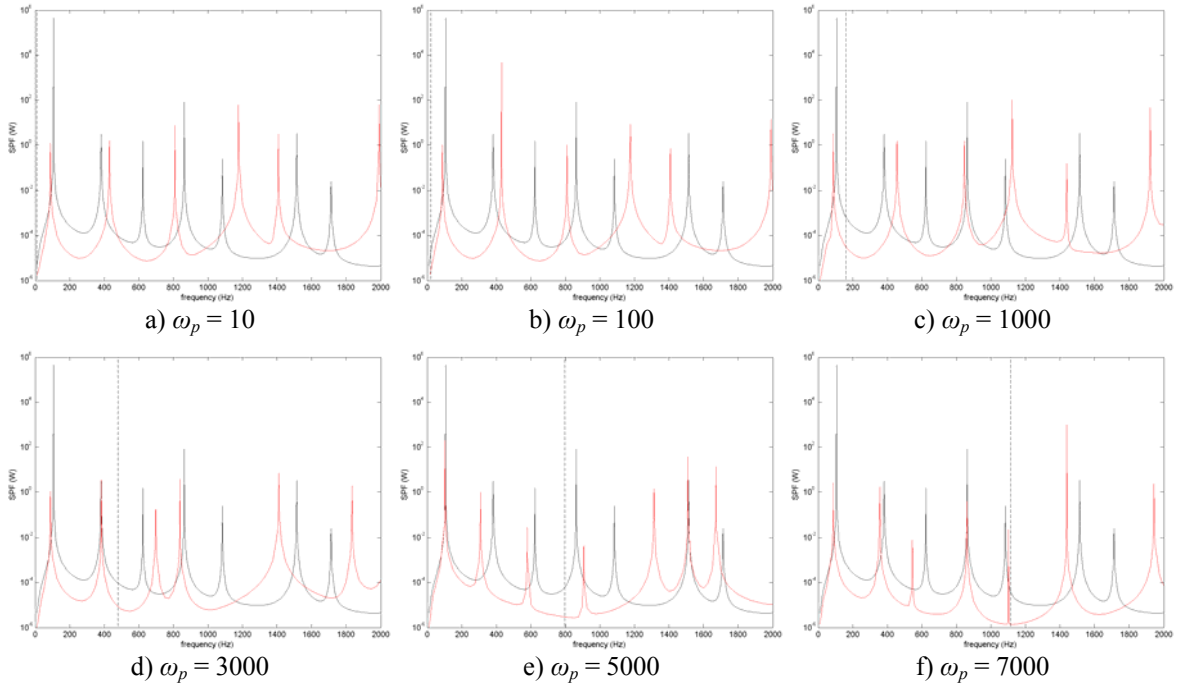

Figure 9. Initial and optimized frequency responses, uniformly distributed pressure loading (ω_p expressed in rad/s). Vertical line indicates the position of the prescribed forcing frequency ω_p in Hz.

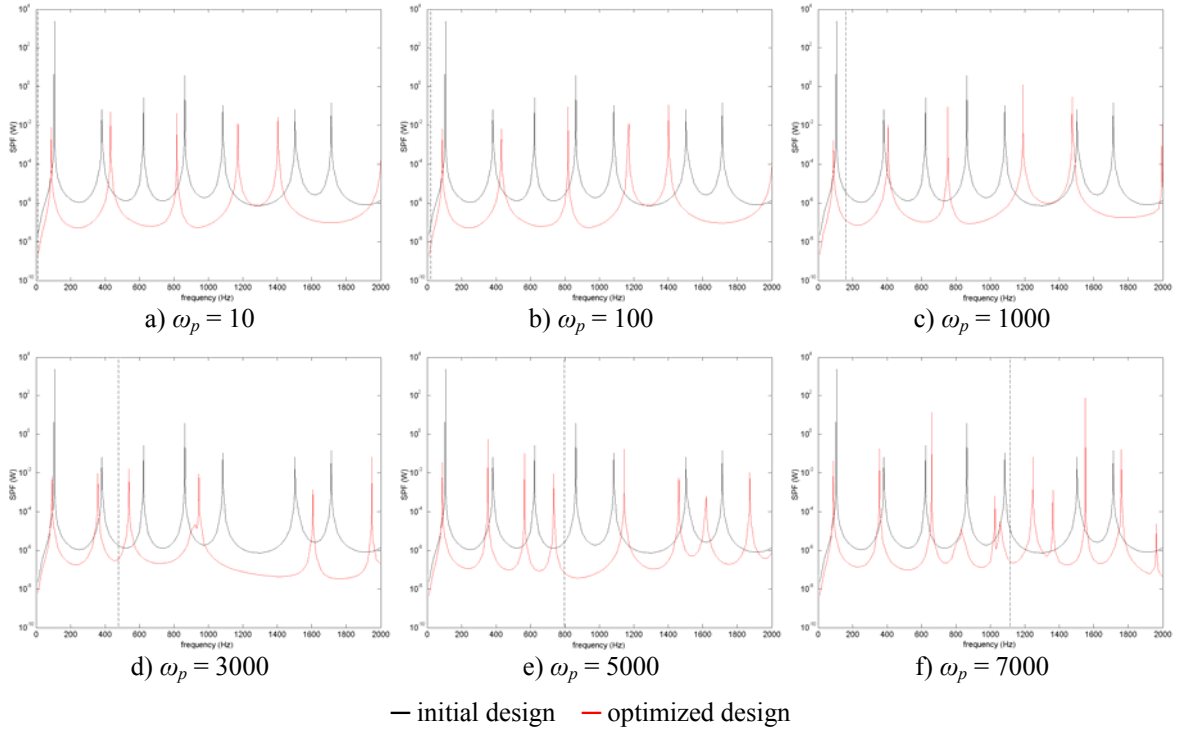

Figure 10. Initial and optimized frequency responses, centred point force loading (ω_p expressed in rad/s). Vertical line indicates the position of the prescribed forcing frequency ω_p in Hz.

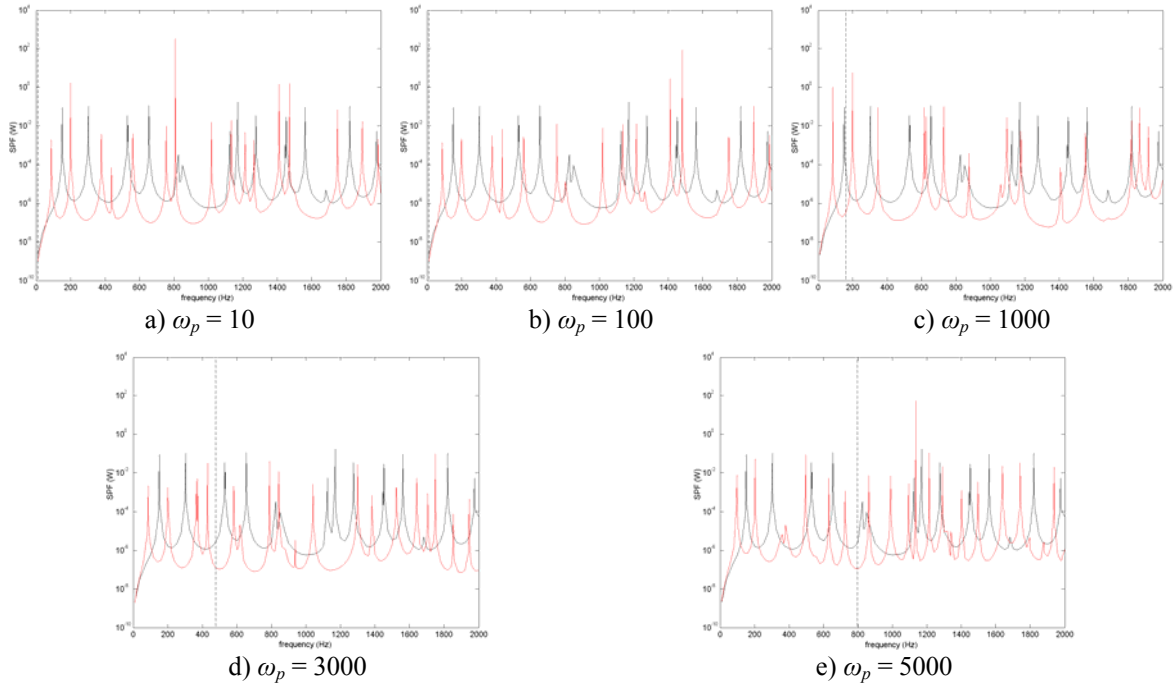

Figure 11. Initial and optimized frequency responses, point force loading deviated from centre (ω_p expressed in rad/s). Vertical line indicates the position of the prescribed forcing frequency ω_p in Hz.

Changes to the responses include the shift, suppression and introduction of peaks, the later being very significant for the case of a point force deviated from the centre of the plate, in which case the sound power flow spectra gets denser after the optimization (see Fig. 11). The peaks in the vicinities of ω_p may either be pulled towards this frequency or pushed away, depending on both the type of loading and ω_p. Although it is desirable to obtain improvements in a whole given range around the optimization frequency, depending on the excitation frequencies to which the structure will be subjected, that may not be verified.

Future work including structural damping and RMS (Root Mean Square) measures should reinforce the presented optimization results.

5.2. Maximization of the Sound Power Flow

Sound radiation increases of 10%, 7.5%, 2057%, 750%, 111% and 118% were obtained for the prescribed forcing frequencies ω_p = 10, 100, 1000, 3000, 5000 and 7000 rad/s, respectively, for the case of a uniformly distributed pressure loading. All optimized design sets fully consisted of the softer material, meaning that the volumetric density of stiffer material is $\rho_e = 0.0$ for all the elements of the domain, reducing the structure's stiffness to a minimum.

6. CONCLUSIONS AND FURTHER RESEARCH

Topology optimization of a bi–material structure with respect to structure–borne radiation has been investigated. The process based on the combination of both F.E. software and MatLab algorithms and here presented works well, leading to reductions of 32% to 99% of the sound power flow, with around 30% or 40% of stiffer material for most cases (see section 5.1); and maximizations from 7.5% to 2057% were also achieved (as referred in section 5.2), with the new design sets fully composed of the softer material.

Most optimized topologies for the minimization of the sound power flow resulted in black–and–white design sets as desired, that is, with no grey color elements consisting of intermediate materials. For the point force loading deviated from the centre at a forcing frequency of 7000 rad/s, a considerable amount of grey elements persisted. Since the iterative process converged to a solution which actually increases the sound power flow, a design set leading to a radiation reduction of 92%, was therefore considered. For these and higher frequencies more time is needed for the optimization, which gets increasingly oscillatory. Use of Trefftz approaches is mentioned for these cases by several authors (Rejlek *et al*., 2007).

Topology complexity depends not only on the type of loading, but also on the prescribed loading frequency; it strongly increases for point forces deviated from the centre of the plate and/or higher frequencies, situations for which the optimization may lead to manufacturability–related issues associated to the presence of 'point masses' and

intermediate materials. Such inconvenience may be avoided by introducing additional algorithms (mesh-independency or perimeter control algorithm, etc.) or constraints to the existing optimization process. Finite element mesh refinements, i.e., increase of the number of finite elements in order to add more detail, shall also be taken into account.

The optimized topologies have both a positive and negative impact across the considered range of frequencies ([1, 2000] Hz). Changes to the sound power flow spectra include the shift and modification of the number of peaks, the later being very significant for the case of a point force deviated from the centre of the plate. Nonetheless, the objective of reducing the sound radiation at the specific forcing frequencies was reached.

Currently a possible extension of the method here presented to the structural optimization with respect to the noise generated by flow–induced vibrations is being investigated. Such vibrations are common and the resulting noise may be felt in everyday situations, such as inside automobiles or an aircraft cabin during flight. The Corcos model, which describes well the pressure fields under separated/reattached and turbulent flows, is being used for studying the response of the plate-like structure to such, allowing the calculation of its spatially averaged mean square velocity v_{av} (details on this model may be found in work by Park *et al*., 2003). Future work also includes introduction of structural damping to reinforce the results.

7. ACKNOWLEDGEMENTS

This work received support from FCT through the project POCTI/EME/ 44728/2002 (MMN), FEDER and IDMEC-IST. The authors would like to thank Prof. Krister Svanberg from the Royal Institute of Technology, Stockholm, for providing his MatLab version of the MMA optimizer.

8. REFERENCES

ANSYS Manual: Theory Reference, 2004, Ansys Release 9.0, USA, ANSYS, Inc.

Bendsøe, M. P. and Sigmund, O., 1999, "Material Interpolation Schemes in Topology Optimization", Archive of Applied Mechanics 69, pp. 635–654.

Bös, J., 2006, "Numerical Optimization of the Thickness Distribution of Three-Dimensional Structures with Respect to their Structural Acoustic Properties", Struct Multidisc Optim 32, pp. 12–30.

Carvalho, M., Vale, J. L., Pinheiro, L. T. and Neves, M. M., 2006, "Techniques Adopted in Integrating Structural Analysis with Numerical Optimization", 5th International Conference on Mechanics and Materials in Design.

Constans, E. W., Koopmann, G. H. and Belegundu, A. D., 1998, "The Use of Modal Tailoring to Minimize the Radiated Sound Power of Vibrating Shells: Theory and Experiment", Journal of Sound and Vibration 217(2), pp. 335–350.

Herrin, D. W., Martinus, F., Wu, T. W. and Seybert, A. F, 2006, "An Assessment of the High Frequency Boundary Element and Rayleigh Integral Approximations", Applied Acoustics 67, pp. 819–833.

Luo, J. and Gea, H. C., 2003, "Optimal Stiffener Design for Interior Sound Reduction Using a Topology Optimization Based Approach", Journal of Vibration and Acoustics 125, pp. 267–273.

Ming, R. S., Pan, J., Norton, M. P. and Teh, M., 2000, "The Passive Control of Tonal Sound Radiation from Vibrating Structures", Applied Acoustics 60, pp. 313–326.

Olhoff, N. and Du, J., 2007, "Minimization of Sound Radiation from Vibrating Bi-Material Structures using Topology Optimization", Struct Multidisc Optim 33, pp. 305–321.

Park, J., Siegmund, T. and Mongeau, L., 2003, "Analysis of the Flow-Induced Vibrations of Viscoelastically Supported Rectangular Plates", Journal of Sound and Vibration 261, pp. 225–245.

Rejlek, J., Pluymers, B., Diwoky, F., Hepberger, A., Priebsch, H.-H. and Desmet, W., 2007, "Validation of the Wave Based Technique for the Analysis of 2D Steady-State Acoustic Radiation Problems", in: Maia, N. M. M.; Silva, J. M. M., Ribeiro, A. M. R.; Foutul, M. (eds.), Proceedings of International Conf. on Engineering Dynamics ICED2007 (held in Carvoeiro, Portugal), paper 1066 in CD of Proceedings.

Svanberg, K., 1987, "The Method of Moving Asymptotes – A New Method for Structural Optimization", International Journal for Numerical Methods in Engineering 24 (2), pp. 359–373.

9. RESPONSIBILITY NOTICE

The authors are the only responsible for the printed material included in this paper.